Effect of Plate Manipulators on Coherent Structures in a Turbulent Boundary Layer

Candace E. Wark,* Ahmed M. Naguib,† and Hassan M. Nagib‡
Illinois Institute of Technology, Chicago, Illinois 60616

An experimental investigation was carried out to examine the effects of manipulator blades on the Reynolds-stress production process in the log layer of a turbulent boundary layer. A three-dimensional sampling grid was used to investigate the effect of manipulators on the ensemble-averaged velocities and pseudoinstantaneous distributions of the structures associated with Reynolds-stress producing events detected at the wall over the Reynolds number range $3400 < Re_\theta < 5200$. The effect of manipulators on the ejection frequency for $3000 < Re_\theta < 10{,}000$ was found to be small. Furthermore, a reduction of the three-dimensional structure was observed only for the larger scales associated with the production process, and a "return" to conditions equivalent to a regular boundary layer was documented over approximately 100 boundary-layer thicknesses downstream of the manipulators. The results suggest that the larger (outer) structures of boundary layers play only a partial role in the wall process and that this production process can be incipiently generated and self sustained.

Nomenclature

c = length of manipulator in streamwise direction
$D(t)$ = detection function
f = measured ejection frequency
f_{acq} = acquisition frequency
f_c = corrected ejection frequency
f_c^* = corrected normalized ejection frequency
k_Q = threshold for quadrant technique
k_x = threshold for streamwise wall-shear stress technique
L_u = threshold for u-level technique
N = total number of samples in a time series
$Q2$ = Reynolds-stress second quadrant event
$Q4$ = Reynolds-stress fourth quadrant event
Re_x = Reynolds number based on streamwise distance from leading edge of test plate, $= U_\infty x/\nu$
Re_θ = Reynolds number based on momentum thickness, $= U_\infty \theta/\nu$
$R_{\tau_x u}$ = space-time correlation between streamwise wall-shear stress and streamwise velocity
s = streamwise distance between leading edge of manipulator blades in tandem configuration
T^+ = positive streamwise shear stress event
T^- = negative streamwise shear stress event
t_s = time period between samples, $= 1/f_{acq}$
U_∞ = freestream velocity
u' = fluctuating component of streamwise velocity
u_τ = friction velocity
$\langle u \rangle$ = conditionally averaged streamwise velocity, $= \overline{D(t)u'(t)}/\overline{D(t)}$
$\langle v \rangle$ = conditionally averaged normal velocity, $= \overline{D(t)v'(t)}/\overline{D(t)}$
v' = fluctuating component of normal velocity
x^+ = nondimensional streamwise coordinate, $= xu_\tau/\nu$
x_m = streamwise location as measured from the leading edge of the test plate to the leading edge of the upstream manipulator blade
y^+ = nondimensional normal coordinate, $= yu_\tau/\nu$
z^+ = nondimensional spanwise coordinate, $= zu_\tau/\nu$
δ_m = boundary-layer thickness at leading edge of manipulator blades
Δu = average of $\langle u \rangle$ over $5x^+$ and $11y^+$ positions
θ = momentum thickness
ν = kinematic viscosity
ξ = nondimensional distance from manipulator blades, $= (x - x_m)/\delta_m$
τ_x = streamwise shear stress

Introduction

Background

THE structure of the turbulent boundary layer has been studied by numerous investigators. The studies focus mainly on wall-layer streaks,[1-3] hairpin eddies,[4,5] and large coherent structures,[6-8] with emphasis on their relation to the Reynolds-stress production process (commonly referred to as the bursting process). The bursting process has been visually observed to extend to the logarithmic region, and although some discrepancy still exists, the bursting frequency is thought to scale with inner layer variables.[7-10] However, large coherent motions scaling with the boundary-layer thickness have been shown to be important to the dynamics of the turbulent boundary layer.[7,8]

A link between the outer flow and wall events is evident by the works of Corke et al.[11] and Plesniak and Nagib[12] where it was shown that flat-plate manipulator blades placed in the outer region of the boundary layer had a clear effect on the dynamics of the near-wall region as well as impacting the integral quantities. However, the nature of the link is not evident. Corke et al.,[11] using a "matched filtering" technique, determined that the burst frequency increased for a manipulated boundary layer with a skin-friction reduction of approximately 30%. Coughran and Bogard,[13] using the u-level detection technique, observed a 7% decrease in ejection frequency and a 4% decrease in burst frequency. Since the

Presented as Paper 89-1010 at the AIAA 2nd Shear Flow Control Conference, May 13-16, 1989; received May 26, 1989; revision received Dec. 6, 1989; accepted for publication Dec. 20, 1989.

*Assistant Professor, Fluid Dynamics Research Center. Member AIAA.
†Graduate Research Assistant, Fluid Dynamics Research Center. Student Member AIAA
‡Rettaliata Professor and Director, Fluid Dynamics Research Center. Member AIAA.

wall-shear stress was also reduced for the manipulated boundary layer, the normalized ejection frequency was approximately equivalent to that for the regular boundary layer.

Possible reasons for the discrepancies between the two investigations could result from the different detection schemes used, from the value for u_τ used in the normalization of the dimensional ejection frequency, or from the geometric conditions of the manipulators for the investigations. It has been shown that the local skin friction depends strongly upon several geometrical parameters.[12] Therefore, when studying the bursting process in this modified flow condition, one should expect the alteration of the bursting process to also be sensitive to the exact setup of the blades.

Motivation

The motivation for the present investigation was threefold: 1) to determine the effect of manipulator blades on the ejection frequency, 2) to investigate the effect on the spatially-coherent structures in a turbulent boundary layer, and 3) based on results from investigations toward the second motive, to suppress the coherent structures such that their redevelopment to conditions comparable to those for a regular boundary layer could be documented and investigated.

Experimental Equipment and Procedure

The measurements were performed in the Mark V. Morkovin wind tunnel at the Illinois Institute of Technology. The tunnel is a closed-return wind tunnel with a series of honeycomb and screens that provide a turbulence intensity in the test section of less than 0.1% for speeds up to 35 m/s. The test section is 0.61 m × 0.91 m with a length of 5.88 m. The test plate is machined from aluminum and is located at a height of 30 cm from the floor of the test section. Sandpaper (24 grit), 20 cm in length, is placed on the test plate directly downstream from the leading edge of the test plate to act as a fixed transition trigger. The mounting of the sandpaper is such that the substrate is flush with the upper surface of the test plate. A flexible ceiling allowed for a zero-pressure gradient condition in the test section.

Two types of measurements were acquired during this investigation. To address the question of appropriate scaling, the first type of measurement was performed over a large Reynolds number range at several vertical positions in the boundary layer. A single-sensor hot wire was used to acquire data at heights corresponding to $y^+ = 15$, 25, 40, 55, and 110. In addition an X-wire probe was used for $y^+ = 55$, 110, 165, and 220. Three freestream velocities with four streamwise locations gave the Reynolds number range of $3000 < Re_\theta < 10{,}000$. A total of 409,600 points per wire were acquired at 12,000 Hz giving a record length of 34 s. The preceding measurements were performed in both regular and flat-plate manipulated boundary layers. The local skin friction was obtained for a regular boundary layer using both a clauser fit to the mean velocity data and a momentum balance approach. The resulting skin friction differed by less than 2% for these two approaches. For the manipulated boundary layer, the local skin friction and net drag reduction were measured using the momentum balance approach. It is pertinent to note at this point that although the net drag reduction using a momentum balance approach is subject to strong criticism, it is well accepted that significant local skin-friction reduction is achieved. Also, flow visualization results of Corke et al.[11] show a clear effect upon the large-scale boundary-layer structures with manipulation. The latter two points are motivating factors behind this investigation.

For all cases listed in Table 1, the second type of experiment included the measurement of the streamwise and normal velocity (u,v) and the streamwise wall-shear stress (τ_x). Included in this second type are three sets of measurements to be described as follows. The u-v probe was placed at various locations in the boundary layer with respect to the wall-shear probe. The wall-shear sensor consists of a hot wire flush mounted with the top surface of a Plexiglas plug, which was covered with a material having a very low heat conductivity (Ardyl). The rms value of the streamwise wall-shear stress was approximately 22% of the mean value. This is lower than that found by Alfredsson et al.[14] They report a value of 40% of the mean for a hot-wire, wall-shear stress sensor in air flow. The major difference in the rms value between the two investigations is most probably caused by the poorer spatial resolution of the present probe. Another difference is that Alfredsson et al.[14] used an overheat ratio of 1.3 vs the present overheat ratio of 1.6; although, this would not seemingly explain the difference. The wall-shear stress was only used as a detection function to compare the large-scale, three-dimensional structure associated with a Reynolds-stress producing event, between regular and manipulated boundary layers. The wall-shear stress was not used to determine the frequency of "bursting"; therefore, this discrepancy in the rms value of the streamwise wall-shear stress will not affect the present results and conclusions. The wall plug could be positioned at three downstream positions 251, 335, and 386 cm from the leading edge of the test plate.

All hot wires were made from 4-μm-diam tungsten wire. The wires were plated with a copper sulfate solution except for a sensing length of approximately 0.75 mm. This sensing length (l) corresponds to a nondimensional length (l^+) in wall units of $18.3 < l^+ < 33$ for $3000 < Re_\theta < 10{,}000$.

Measurements were obtained at 220 spatial positions of a three-dimensional sampling grid for seven of the ten cases in Table 1. The freestream velocity for all cases investigated is $U_\infty = 11$ m/s. Three regular boundary-layer cases were used in the first set: 1) $Re_\theta = 3570$ (hereafter referred to as R1), 2) $Re_\theta = 4620$ (R2), and 3) $Re_\theta = 5120$ (R3). The downstream distance from the leading edge of the test plate is 251, 335, and 386 cm, respectively. In the second set, three cases for an "upstream" manipulated boundary layer were also investigated at the same downstream positions: 1) $Re_\theta = 3670$ (M1), 2) $Re_\theta = 4360$ (M2), and 3) $Re_\theta = 4870$ (M3). The upstream manipulated case refers to two thin (0.127-mm) flat blades in a tandem configuration.[12] The leading edge of the upstream blade is located at $x = 91$ cm from the leading edge of the test plate. The blades are placed at a height in the boundary layer of $h/\delta_m = 0.7$, the streamwise spacing between the leading edge of the two blades is $s/\delta_m = 12$, and the nondimensional length of the manipulator in the flow direction is $c/\delta_m \approx 1.8$. The measurement locations of $x = 251$, 335, and 386 cm correspond to the nondimensional distance from the manipulator blades $\xi = (x - x_m)/\delta_m$ of 63 (M1), 96 (M2), and 116 (M3), respectively.

The local skin friction and momentum thickness evolution downstream of the blades is shown along with the results for

Table 1 Relevant parameters for cases investigated

Case	R1	R2	R3	M3′	M1	M2	M3	D1	D2	D3
Re_θ	3570	4620	5120	5580	3670	4360	4870	4650	4650	4650
ξ	——	——	——	20	63	96	116	3.8	5.4	7.1
h/δ_m	——	——	——	0.5	0.7	0.7	0.7	0.1	0.1	0.1
s/δ_m	——	——	——	7.0	12.0	12.0	12.0	——	——	——
c/δ_m	——	——	——	1.0	1.8	1.8	1.8	3.0	3.0	3.0

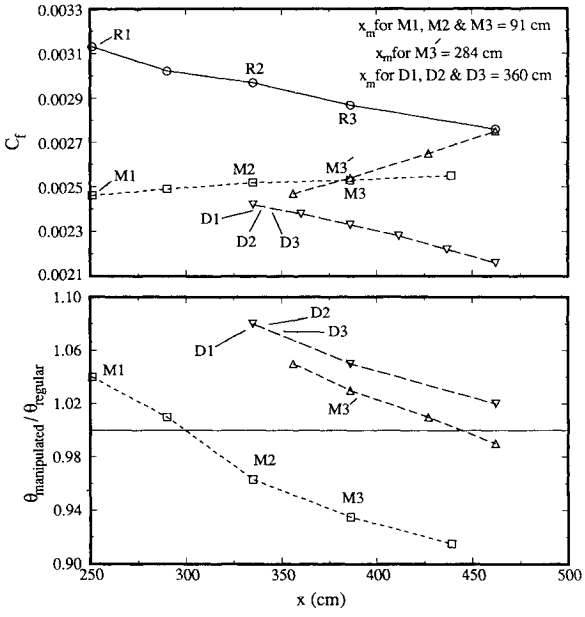

Fig. 1 Skin friction and momentum thickness development downstream from the various manipulator configurations compared to conditions for a regular boundary layer.

a regular boundary layer in Fig. 1. For a zero-pressure gradient boundary layer, the amount of drag reduction achieved is related to the ratio between the momentum thickness growth of the manipulated boundary layer to that of a regular boundary layer. For case M1, the local skin friction is reduced by approximately 22% (top of Fig. 1); however, there is no net drag reduction by this downstream distance ($\theta_{\text{manipulated}}/\theta_{\text{regular}} > 1.0$ as shown in the bottom of Fig. 1). The local skin-friction reduction decreases for M2 and M3, whereas a drag reduction of approximately 4% and 6.5% is achieved by this location on the test plate.

During the second set of experiments, measurements were also obtained with the manipulator blades placed at $x = 284$ cm from the leading edge of the test plate ($h/\delta_m = 0.5$, $s/\delta_m = 7$, $c/\delta_m \approx 1$). The measurement location was at $x = 386$ cm downstream from the leading edge of the test plate, this results in an $Re_\theta = 5580$ and $\xi = 20$ (M3′). The skin-friction reduction for M3′ was approximately 14% (see Fig. 1). At this measurement location, there was no net drag reduction; nevertheless, by the end of the test plate, the momentum thickness for the manipulated boundary layer was slightly less than that for a regular boundary layer.

The three-dimensional sampling grid, which was repeated for each of the preceding seven cases, consisted of the simultaneous measurement of the streamwise wall-shear stress at $(x^+,y^+,z^+) = (0,0,0)$ and the streamwise velocity at 220 spatial sampling points: 5 streamwise ($x^+ = -440$, 0, 440, 880, and 1320), 11 normal ($y^+ = 55$ to 605, $\Delta y^+ = 55$), and 4 spanwise ($z^+ = 0$, 110, 220, and 330) positions. The shear sensor was used to detect a T^+ or a T^- event as described below. The sampling rate ($1/t_s = 5612$ Hz) was such that $t_2^+ = t_s u_\tau^2/\nu = 2$, and 204,800 points per wire were recorded over 36.5 s.

Finally, for the third set of experiments (cases D1, D2, and D3), an X-wire probe, which was positioned at various locations with respect to the wall-shear probe, was oriented to measure the streamwise and normal (u,v) components of the velocity. Data were taken at 4 streamwise, 11 normal, and 5 spanwise positions with respect to the shear sensor, ($x^+ = -440$, 0, 440, and 880), ($y^+ = 55$ to 605, $\Delta y^+ = 55$), ($z^+ = 0$, 110, 220, 330, and 440). For these three manipulated boundary-layer cases, the blades were positioned at a relatively low height in the boundary layer in a stacked rather than tandem configuration: the bottom blade was placed at $y^+ = 150$ ($h/\delta_m = 0.1$), and the top blade was placed at $y^+ = 440$ ($h/\delta_m = 0.3$). For both blades $c/\delta_m \approx 3$. The sampling grid was relatively close to the blades ($\xi = 3.8$, 5.4, and 7.1). Although the local skin friction was reduced by approximately 20% downstream of the blades, no net drag reduction was achieved by the end of the test section (see Fig. 1).

Data Processing

Space-Time Correlations

The space-time correlation between two fluctuating quantities α and β is defined by

$$R_{\alpha\beta}(x^+,y^+,z^+,t^+) = \frac{\overline{\alpha'(0,0,0,0)\beta'(x^+,y^+,z^+,t^+)}}{\sqrt{\overline{\alpha'^2}}\sqrt{\overline{\beta'^2}}}$$

The $R_{\tau_x u}(x^+,y^+,z^+,t^+)$ are presented for the various regular and manipulated boundary-layer conditions investigated.

Detection of Events and Conditional Averaging

Three common schemes are employed to detect events associated with Reynolds-stress production: quadrant, u level, and shear stress methods. The detection functions are given below.

The u level

$$D(t) = \begin{cases} 1 & \text{if } u'(t) < L_u u_{\text{rms}} \\ 0 & \text{otherwise} \end{cases}$$

Quadrant

$$Q4\ D(t) = \begin{cases} 1 & \text{if } u'(t) > 0 \text{ and } u'(t)v'(t) < k_Q u_{\text{rms}} v_{\text{rms}} \\ 0 & \text{otherwise} \end{cases}$$

$$Q2\ D(t) = \begin{cases} 1 & \text{if } u'(t) < 0 \text{ and } u'(t)v'(t) < k_Q u_{\text{rms}} v_{\text{rms}} \\ 0 & \text{otherwise} \end{cases}$$

Shear stress

$$T^+\ D(t) = \begin{cases} 1 & \text{if } \tau_x' > k_x \tau_{x\,\text{rms}}' \\ 0 & \text{otherwise} \end{cases}$$

$$T^-\ D(t) = \begin{cases} 1 & \text{if } \tau_x' < k_x \tau_{x\,\text{rms}}' \\ 0 & \text{otherwise} \end{cases}$$

Based upon a chosen detection scheme for a given time series, the frequency of occurrence at the detection point of a particular event (f) is given by

$$f = \frac{\text{no. of detections}}{\text{time period}} = \frac{\sum_{i=1}^{N} D_i(t)}{Nt_s} = \frac{\sum_{i=1}^{N} D_i(t)}{N1/f_{\text{acq}}} = f_{\text{acq}}\left[\frac{\sum_{i=1}^{N} D_i(t)}{N}\right]$$

The correction on the measured frequency to account for spatial-averaging effects of the sensor, as introduced by Blackwelder and Haritonidis,[9] is given by $f_c = f[1.0 + (l^+/l_0^+)^2]^{0.5}$ where f_c is the corrected frequency, l^+ is the nondimensional sensor length ($l^+ = lu_\tau/\nu$), and $l_0^+ = 20$ was determined to produce optimal results.

Bogard and Tiederman[15] showed that several ejections could be grouped into a single burst; therefore, proper counting of bursts is done by analyzing the probability distribution of time between ejections (T_E). The same method, as used by Bogard and Tiederman[15] and Luchik and Tiederman,[16] was used to determine the appropriate time delay to leave between ejections before counting another burst.

The sensor-length correction for an X-wire probe is not as straightforward as for the single-sensor probe. The present authors are not aware of any systematic investigation to determine the spatial-averaging correction for X-wire probes. Therefore, the correction to the frequency results shown using an X-wire probe was determined in the following manner. Data were acquired at $y^+ = 55$ and 110 using both a single-sensor and an X-wire probe. The frequency of variable interval time averaging (VITA) and u-level events was determined for the single-sensor data using the correction scheme described earlier. The correction to the frequency for the X-wire data was determined such that the corrected frequency for the X-wire data was equal to the corrected frequency for the single-sensor data. This resulted in a l^+ value in $f_c = f[1.0 + (l^+/l_0^+)^2]^{0.5}$ for the X-wire results, which was 10% larger than the corresponding value for the single probe with an equivalent sensing length.

Three-Dimensional Probability Density Functions

To investigate the spatially coherent structures associated with a detection of an ejection using the shear stress technique, the average fluctuating velocities in a three-dimensional grid, measured with the X-wire (u,v) probe about the detection point, are calculated ($\langle u \rangle$ and $\langle v \rangle$) by the following relations.

$$\langle u \rangle = \frac{\overline{D(t)u'(t)}}{\overline{D(t)}} \qquad \langle v \rangle = \frac{\overline{D(t)v'(t)}}{\overline{D(t)}}$$

The above results are all based upon ensemble-averaged quantities for the perturbation velocity. Knowledge of the instantaneous field is more useful and interesting as compared to the mean field; however, the associated experimental limitations are numerous. To extract information regarding the instantaneous field, conditional probability density functions (pdfs) were calculated as described below.

The approach taken for the present results is based on the pdfs for the time between an event recognized at the detection point and an event observed at the mapping probe. These pdfs were evaluated for every point of the sampling grid. A time delay between an event occurring at the detection probe and the mapping probe was chosen, and then the probability value was assigned a color (see the color bar on each figure). Note: The background or random probability of detecting a $Q4$ event is subtracted from the pdfs at every grid point.

Discussion of Results

Ejection Frequency and Detection of Events

It is evident when comparing the implementation of the various detection schemes that the outcome of the results will be highly dependent on the user-specified threshold parameters. However, if the various schemes are detecting the bursting process accurately, then features such as the qualitative trend with Reynolds number should be similar between detection schemes.

The results in Fig. 2 represent the effect of manipulators (plotted in closed symbols) on the nondimensional ejection frequency as detected using the quadrant ($k_Q = -3$) (X-wire from $55 < y^+ < 220$) and u-level ($L_u = -1.3$) methods (single wire was used from $15 < y^+ < 110$ and X-wire from $55 < y^+ < 220$). The u_τ used for normalizing the ejection frequency of the manipulated boundary layer was that obtained for the regular boundary layer at the same Re_x. The ejection frequency shown is the result of averaging (for a given y^+) over the 12 measurement locations: three freestream velocities with four streamwise locations for a Reynolds number range of $3000 < Re_\theta < 10{,}000$. The ξ values range from $40 < \xi < 120$. The differences between the regular and manipulated boundary layer exhibit no clear trend with Reynolds number or streamwise location; thus, the results were averaged over all measurement postions. For the u-level comparison, a decrease of ejection frequency at $y^+ = 15$ for the manipulated boundary layer is seen. However, there is virtually no effect on the frequency for $25 \le y^+ \le 110$. When using the $Q2$ method, an increased effect with increasing y^+ is observed. However, conclusions should be made with caution regarding the effect of manipulators on ejection frequency. In the same laboratory,[8] a qualitatively different effect (albeit small) was seen for the same range of Reynolds numbers at $y^+ = 55$. Also, the results of Coughran and Bogard[13] agree with the present results for $y^+ = 15$. Their results show a decrease of u-level ejection frequency for $19 \le y^+ \le 55$ when normalized with the local u_τ. As mentioned previously, the present results use the u_τ values obtained for the regular boundary layer for normalization. In summary as mentioned in the Introduction, the effect of manipulators on the ejection frequency is small and very sensitive to experimental setup. It was therefore decided to investigate more thoroughly the effect of the manipulators on the three-dimensional structures associated with Reynolds-stress production.

The ensemble-averaged perturbation velocity $\langle u \rangle$, (average streamwise velocity associated with a detection at the wall) at a measurement location is averaged over all streamwise (x^+) and normal (y^+) measurement locations for a given spanwise location (z^+). The result (Δu) is shown in Fig. 3 as a function

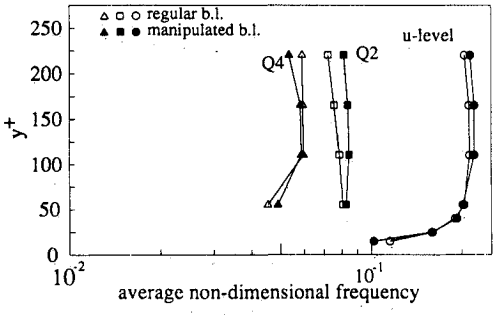

Fig. 2 Average corrected ejection and sweep frequency of occurrence as obtained from u-level and quadrant detection schemes, as a function of height, averaged over $3000 < Re_\theta < 10000$ using mixed scaling.

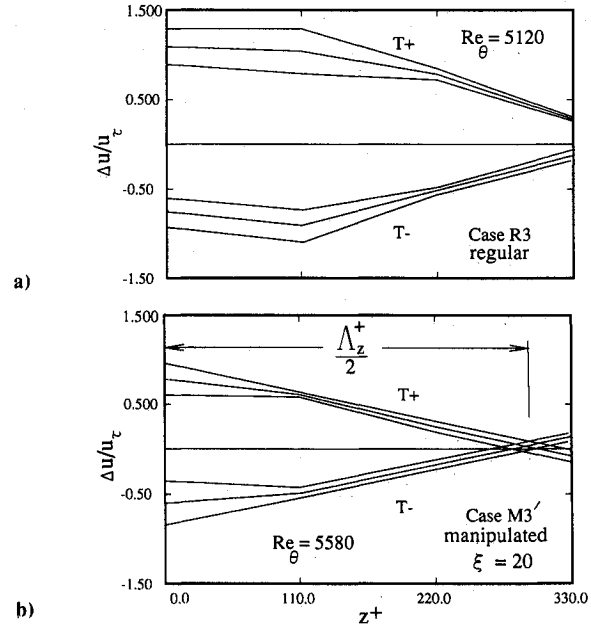

Fig. 3 Spanwise variation of Δu depicting the spanwise extent of the coherent structures for a) a regular boundary layer ($Re_\theta = 5120$) and b) a manipulated boundary layer ($Re_\theta = 5580$, $\xi = 20$ [M3′]).

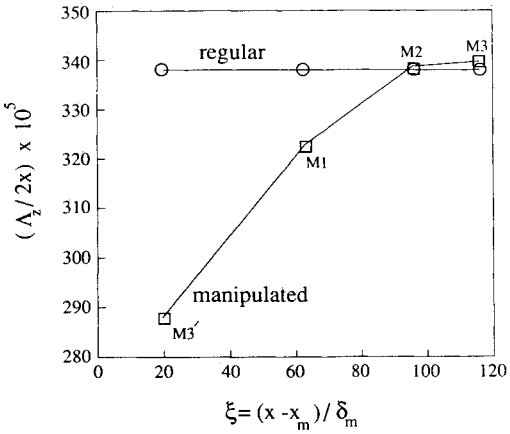

Fig. 4 Variation of the integral measure of the spanwise size of the coherent structures with downstream distance plotted vs normalized distance from manipulator blades, compared to a regular boundary layer.

of z^+ along with two curves that represent plus and minus the standard deviation over the 5 (x^+) and 11 (y^+) locations. The quantity $\Lambda_z^+/2$ is the spanwise location, normalized by inner variables, where $\Delta u/u_\tau = 0$ and gives an indication of the spanwise extent of the ensemble-averaged structure associated with a wall-shear stress detection.

The effect of the blades is clear when comparing Figs. 3a and 3b; specifically, Λ_z is approximately 20% less than for a regular boundary layer at the same Re_x. Figure 4 summarizes all cases investigated and depicts the return of Λ_z to conditions equivalent to a regular boundary layer for $\xi \approx 100$. For $\xi > 100$ not only is Λ_z equivalent to a regular boundary layer, but in addition $\Delta u/u_\tau$ for $z^+ \leq \Lambda_z^+/2$ is equivalent to a regular boundary layer at the same Re_x. We interpret Λ_z as an integral measure of the hierarchy of the Reynolds-stress producing scales in the boundary layer.

At this point, a subsequent investigation was undertaken to examine the link between the change of Λ_z with ξ. Repeating the experiment for $2 < \xi < 20$ showed no further decrease of Λ_z. To significantly lower Λ_z and affect the velocity field associated with the coherent structures, the blades had to be placed at lower h/δ_m locations. The blades were placed in a parallel configuration as shown in Fig. 5. The effect of placing the blades at lower y^+ values results in an increased reduction in the spatial extent and frequency of events (as follows). The sampling grid was located 3.8 boundary-layer thicknesses downstream of the leading edge of the manipulator blades. The velocity vector maps in the x-y plane result when averaging (at all measurement points) the fluctuating streamwise and normal velocity components associated with the detection of a T^- event ($k_x = -1.9$) at the wall.

For the blade positions of $y^+ = 440$ and 150 (see Fig. 5), measurements were made at two other downstream locations with respect to the manipulators, i.e., $\xi = 7.1$ and 5.4 in addition to $\xi = 3.8$ (cases D3, D2, and D1, respectively). The detection frequency (ejection frequency) of the manipulated boundary layers with respect to a regular boundary layer (f_M/f_R) changes as ξ increases in the following manner:

$$\xi = 3.8 \qquad f_M/f_R = 50\%$$

$$\xi = 5.4 \qquad f_M/f_R = 53\%$$

$$\xi = 7.1 \qquad f_M/f_R = 77\%$$

Space-Time Correlations

The effect of boundary-layer manipulation on the space-time correlations is demonstrated by comparing results of cases M3′, M3, and R3. Figures 6 depict the space-time correlations for the preceding cases at a streamwise offset of $x^+ = 0$ and a normal offset of $y^+ = 55$ for the range of

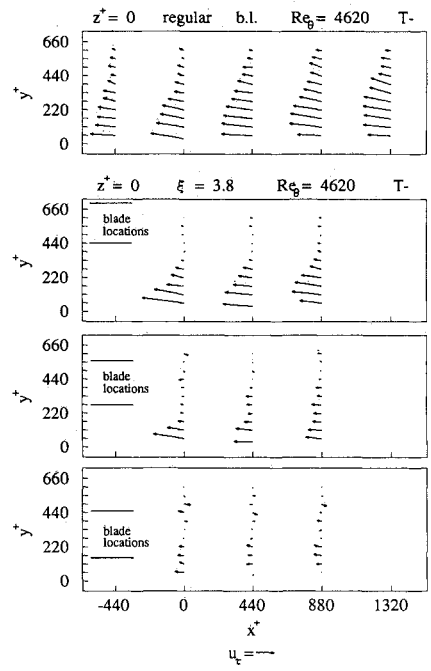

Fig. 5 Velocity vector maps in the x-y plane at $\xi = 3.8$ for a manipulated boundary layer, with blades located as indicated, for the T^- event at $z^+ = 0$, compared with a regular boundary layer.

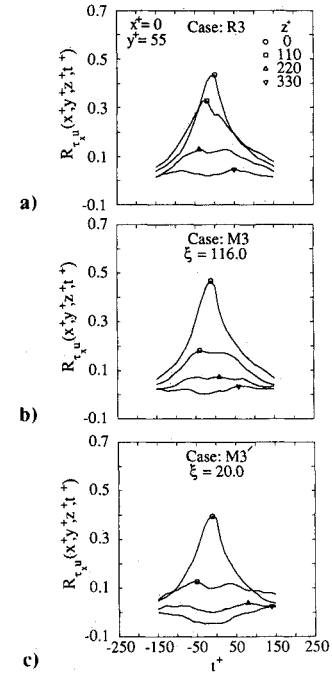

Fig. 6 Temporal dependence of $R_{\tau_x u}$ correlations at $x^+ = 0$ and $y^+ = 55$ as a function of z^+ for a) regular boundary layer ($Re_\theta = 5120$); b) manipulated boundary layer (M3 $Re_\theta = 4870$, $\xi = 116$); c) manipulated boundary layer (M3′ $Re_\theta = 5580$, $\xi = 20$).

spanwise offsets investigated. By comparing Figs. 6a–c, it is noted that the correlation at $z^+ = 0$ is similar for the three cases; whereas, for $z^+ \geq 110$, there is a significant drop in the correlation for the manipulated cases as compared with that for the regular boundary-layer case. This demonstrates a significant effect of manipulators on the spanwise structures in the turbulent boundary layer.

Another important observation from these results is that the maximum magnitude of the correlations at $z^+ = 110$ and 220 for case M3 has not reached that for case R3. However,

as depicted by the results of Nagib et al.[17] discussed earlier, the $\Delta u/u_\tau$ vs z^+ results of turbulence producing events has "relaxed" to regular boundary-layer conditions by $\xi = 116$ (M3) (see Fig. 4). The fact that the correlation values for $z^+ = 110$ and 220 are lower than those for a regular boundary layer suggests that a "full" return to regular boundary-layer conditions has not been achieved by $\xi = 116$. Referring to Fig. 1, one can see that the skin-friction coefficient and the momentum thickness are also not equivalent to a regular boundary layer by $\xi = 116$.

Space-time correlations results for cases D1, D2, and D3 are shown in Fig. 7. The effect on the long-time correlation is observed not only for $z^+ > 0$ but also at $z^+ = 0$ for $\xi = 3.8$. As discussed above, it was this low placement of the blades in the boundary layer ($h/\delta_m = 0.1$) that resulted in a substantial reduction in the magnitudes of the streamwise and normal perturbation velocities (see Fig. 5). By $\xi = 7.1$, the magnitudes of the long-time correlations have approached those for a regular boundary layer in a relatively short distance; nevertheless, a decrease of the magnitudes is still present.

All of the preceding evidence lends support to the observation by Wark[8] that the turbulence producing events are composed of a hierarchy of events with the manipulators (when placed at relatively high heights) acting on the largest of the realizations as indicated by $\Delta u/u_\tau(z^+)$ results. In addition, these large scales take several boundary-layer thicknesses (>100) to return to those comparable to a regular boundary layer. The small scales, however, return or develop over a very short distance.

Three-Dimensional Probability Density Distributions

The results using this statistical approach provide some understanding of the instantaneous three-dimensional field associated with a wall-shear stress detection. Specifically, the probability of a user specified event anywhere in the measurement grid occurring simultaneously with the detection of an event at the wall-shear stress sensor ($x^+ = y^+ = z^+ = 0$) is determined. This is useful in estimating the scales associated with a detection, which can subsequently provide information regarding the distribution or range of scales involved in the ensemble-averaging process. This information may be obtained for any user-specified condition and any parameter value by the postprocessing of the digitially stored boundary-layer data.

Figures 8 and 9 depict the comparison of the probability of observing a $Q2$ or a $Q4$ ($k_Q = 0$) event when detecting a T^- ($k_x = -1.9$) or a T^+ ($k_x = 2.4$) event, respectively, for cases R2, D3, and D1. The probability of observing a $Q2$ event

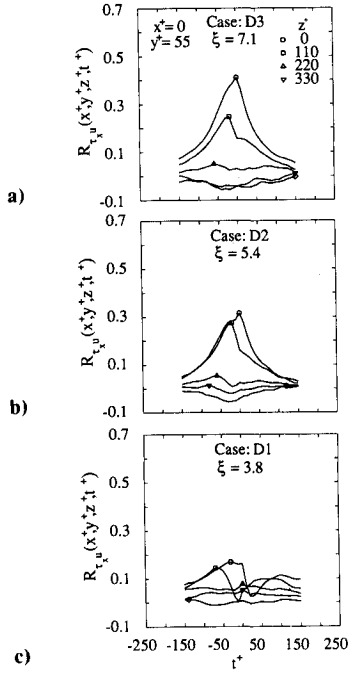

Fig. 7 Temporal dependence of $R_{\tau_x u}$ correlations at $x^+ = 0$ and $y^+ = 55$ as a function z^+ for a) manipulated boundary layer (D3: $Re_\theta = 4650$, $\xi = 7.1$); b) manipulated boundary layer (D2: $Re_\theta = 4650$, $\xi = 5.4$); manipulated boundary layer (D1: $Re_\theta = 4650$, $\xi = 3.8$).

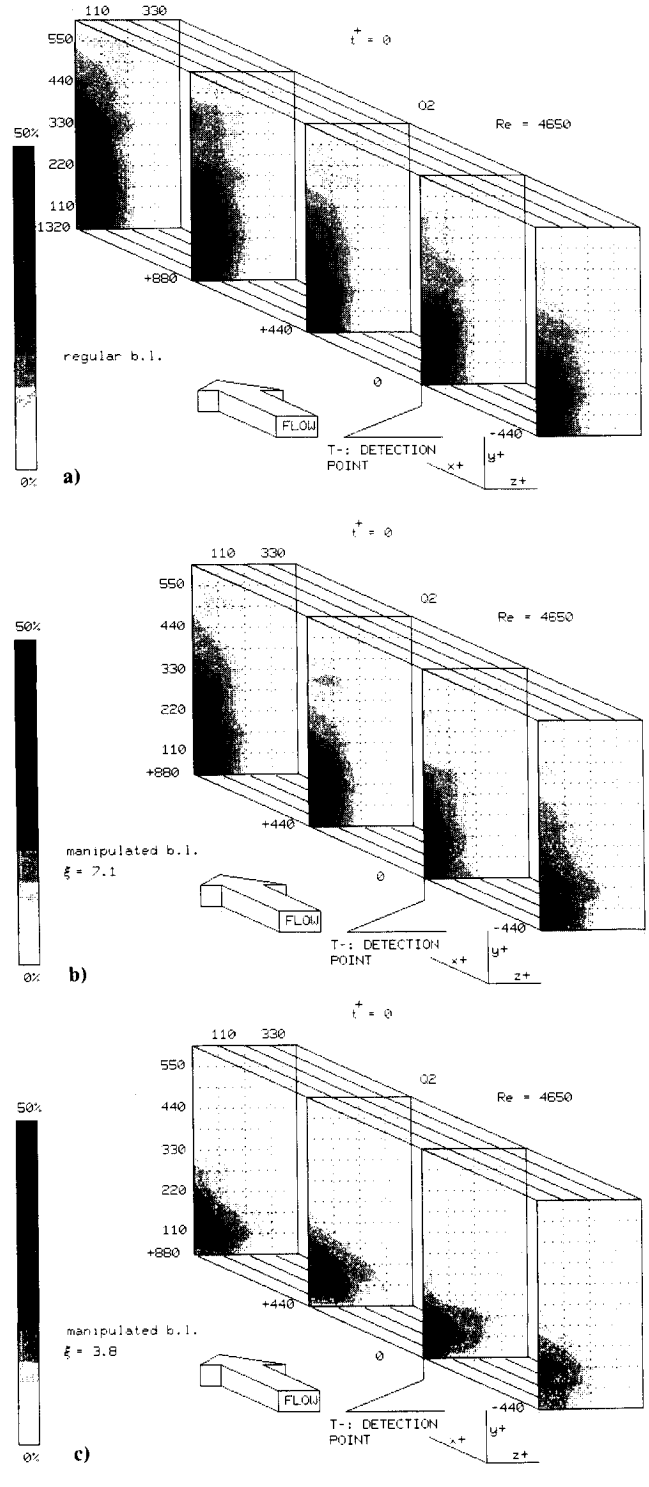

Fig. 8 Three-dimensional spatial presentation of probability of a $Q2$ event ($k_Q = 0.0$) to occur simultaneously with the detection of a strong T^- event at $(x^+, y^+, z^+) = (0,0,0)$ for a) a regular boundary layer ($R2$, $Re_\theta = 4650$); b) a manipulated boundary layer (D3, $Re_\theta = 4650$ and $\xi = 7.1$); c) a manipulated boundary layer (D1, $Re_\theta = 4650$ and $\xi = 3.8$).

when detecting a T^- event for $\xi = 3.8$ is shown in Fig. 8c. The probability is relatively low and confined to a small spanwise and vertical extent from the detection point. As distance from the blades increases to $\xi = 7.1$ (Fig. 8b), both the magnitude of the probability and the sizes of the scales increase. The pdfs for a regular boundary layer at the same Re_x show a further increase in the magnitudes and scales

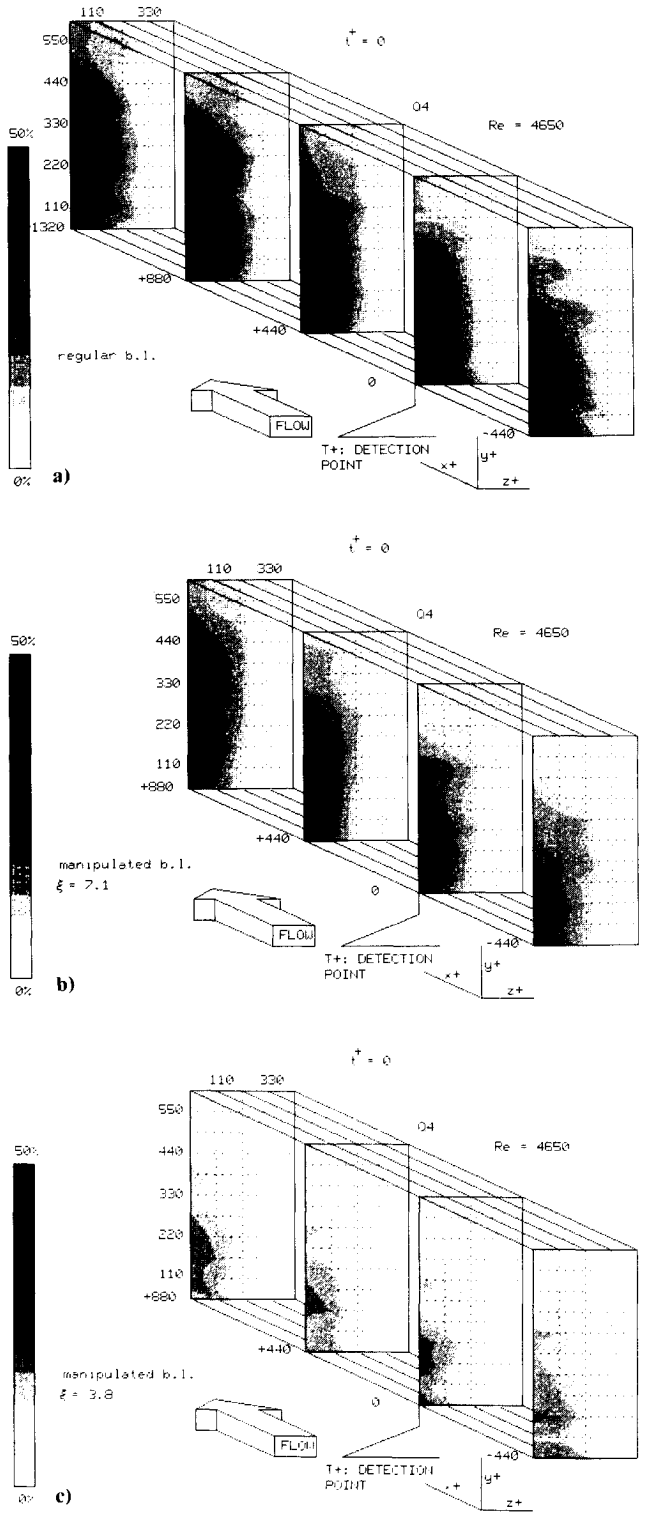

Fig. 9 Three-dimensional spatial presentation of probability of a $Q4$ event ($k_Q = 0.0$) to occur simultaneously with the detection of a strong T^+ event at $(x^+,y^+,z^+) = (0,0,0)$ for a) a regular boundary layer (R2, $Re_\theta = 4650$); b) a manipulated boundary layer (D3, $Re_\theta = 4650$ and $\xi = 7.1$); c) a manipulated boundary layer (D1, $Re_\theta = 4650$ and $\xi = 3.8$).

associated with a T^- detection. This is compatible with the space-time correlations shown in Fig. 7.

The same observations for the pdfs of a $Q4$ event when detecting a T^+ event at the wall can be made for increasing ξ and comparing with the regular boundary layer (see Fig. 9). Again this is good agreement with the correlations of Fig. 7. Overall, the probabilities are larger in magnitude and extend to greater z^+ and y^+ values for the $[T^+, Q4]$ pdfs (see Fig. 9) as compared with the $[T^-, Q2]$ pdfs (see Fig. 8). A more detailed discussion of this is given by Wark.[8]

Conclusions

The effect of manipulators placed at $h/\delta_m > 0.5$ on the frequency of occurrence of events associated with the production process is small, and the qualitative trend is sensitive to the experimental setup of the blades. A more clear effect is observed when studying the three-dimensional spatial structure associated with a detection. When the blades are placed in a configuration such that net drag reduction is realized by the end of the test section ($h/\delta_m > 0.5$), an integral measure of the spanwise extent of the average perturbation velocity field (Λ_z) is reduced by approximately 22% for $\xi = 20$. The length scale Λ_z is observed to increase with increasing ξ and to reach a value equal to that for a regular boundary layer by approximately $\xi = 100$. An interesting observation is made when studying the space-time correlations for the cases investigated. The long-time correlations supplement the Λ_z results in the sense that they show that even though Λ_z returns to conditions equivalent to a regular boundary layer by $\xi = 116$, the long-time correlations for $z^+ < \Lambda_z^+$ exhibit lower values than those for a regular boundary layer. This is consistent with the result that the skin-friction coefficient has also not reached a value equivalent to a regular boundary layer by $\xi = 116$.

Pseudoinstantaneous results provided by the conditional probability density distributions lend further support for the development of scales downstream of the manipulator blades. That is, small-scale structures exhibit a very rapid return (within $\xi < 7.1$) to conditions equivalent to a regular boundary layer. However, as mentioned previously, the largest realizations in the ensemble-averaged structure take several boundary-layer thicknesses ($\xi \approx 100$) to recover to conditions similar to a regular boundary layer.

The mechanisms by which manipulator blades achieve drag reduction are not of course fully explained by the present investigation. However, the results support the suppression mechanisms and their consequences as proposed by the IIT publications, rather than the breakup ideas (large eddy breakup) adopted by NASA workers and followed by many others, or the wake effect concepts suggested by the early Cambridge University work. More significantly, the results reveal that the outer structures of boundary layers may play only a partial role in the wall process and that this production process can be incipiently generated and self sustained. Further discussion of these ideas is provided by Wark and Nagib[18] and Nagib et al.[19]

Acknowledgment

The support of this work was provided by the Air Force Office for Scientific Research under Contract F49620-86-C-0133 monitored by J. McMichael and H. Helin.

References

[1]Kim, H. T., Kline, S. J., and Reynolds, W. C., "The Production of Turbulence near a Smooth Wall in a Turbulent Boundary Layer," *Journal of Fluid Mechanics*, Vol. 50, Nov. 1971, pp. 133–160.

[2]Corino, E. R., and Brodkey, R. S., "A Visual Investigation of the Wall Region in Turbulent Flows," *Journal of Fluid Mechanics*, Vol. 37, June 1969, pp. 1–30.

[3]Smith, C. R., and Metzler, S. P., "The Characteristics of Low-Speed Streaks in the Near Wall Region of a Turbulent Boundary Layer," *Journal of Fluid Mechanics*, Vol. 129, April 1983, pp. 27–46.

[4]Head, M. R., and Bandyopadhyay, P., "New Aspects of Turbu-

lent Boundary Layer Structure," *Journal of Fluid Mechanics*, Vol. 107, June 1981, pp. 297–337.

[5]Perry, A. E., Henbest, S., and Chong, M. S., "A Theoretical and Experimental Study of Wall Turbulence," *Journal of Fluid Mechanics*. Vol. 165, April 1986, pp. 163–199.

[6]Bakewell, H. P., and Lumley, J. L., "Viscous Sublayer and Adjacent Region in Turbulent Pipe Flow," *Physics of Fluids*, Vol. 10, Sept. 1967, pp. 1880–1889.

[7]Guezennec, Y. G., "Documentation of Large Coherent Structures Associated with Wall Events in Turbulent Boundary Layers," Ph.D. Thesis, Illinois Institute of Technology, Chicago, IL, Dec. 1985.

[8]Wark, C. E., "Experimental Investigation of Coherent Structures in Turbulent Boundary Layer," Ph.D. Thesis, Illinois Institute of Technology, Chicago, IL, May 1988.

[9]Blackwelder, R. F., and Haritonidis, J. H., "Scaling of the Bursting Frequency in Turbulent Boundary Layers," *Journal of Fluid Mechanics*, Vol. 132, July 1983, pp. 87–103.

[10]Willmarth, W. W., and Sharma, L. K., "Study of Turbulent Structure with Hot Wires Smaller Than the Viscous Length," *Journal of Fluid Mechanics*, Vol. 142, May 1984, pp. 121–149.

[11]Corke, T. C., Nagib, H. M., and Guezennec, Y. G., "A New View on Origin, Role and Manipulation of Large Scales in Turbulent Boundary Layers," NASA CR-165861, 1982; see also Ph.D. Thesis by T. C. Corke, Illinois Institute of Technology, Chicago, IL, 1981.

[12]Plesniak, M. W., and Nagib, H. M., "Net Drag Reduction in Turbulent Boundary Layers Resulting form Optimized Manipulation," AIAA Paper 85-0518, March 1985; see also M.S. Thesis by M. W. Plesniak, Illinois Institute of Technology, Chicago, IL, 1985.

[13]Coughran, M. T., and Bogard, D. G., "An Experimental Study of the Burst Structure in a LEBU-Modified Boundary Layer, "*Proceedings of the Tenth Symposium on Turbulence*. University of Missouri, Rolla, MO, 1986, pp. 45-1–45-10.

[14]Alfredsson, P. H., Johansson, A. V., Haritonidis, J. H., and Eckelmann, H., "The Fluctuating Wall-shear Stress and the Velocity Field in the Viscous Sublayer," *Physics of Fluids.*, Vol. 31, No. 5, May 1988, pp. 1026–1033.

[15]Bogard, D. G., and Tiederman, W. G., "Burst Detection with Single-Point Velocity Measurements," *Journal of Fluid Mechanics*, Vol. 162, Jan. 1986, pp. 389–413.

[16]Luchik, T. S., and Tiederman, W. G., "Timescale and Structure of Ejections and Bursts in Turbulent Channel Flows," *Journal of Fluid Mechanics*, Vol. 174, Jan. 1987, pp. 529–552.

[17]Nagib, H. M., Wark, C. E., and Guezennec, Y. G., "Documentation of Turbulence Producing Structures in Regular and Manipulated Turbulent Boundary Layers," *Proceedings of the IUTAM Symposium on Turbulence Management and Relaminarisation*, Springer-Verlag, Bangalore, India, Paper No. 1, Jan. 1987.

[18]Wark, C. E., and Nagib, H. M., "Relation Between Outer Structures and Wall-layer Events in Boundary Layers With and Without Manipulation, "*Proceedings of the IUTAM Symposium on Structure of Turbulence and Drag Reduction*, Springer-Verlag, Zurich, Switzerland, July 1989.

[19]Nagib, H. M., Wark, C. E., and Naguib, A. M., "Effects of Blade Manipulators on Turbulence Production and Why They are not LEBU's, *Proceedings of Drag Reduction 89*, Ellis Horwood Limited, Davos, Switzerland, July–Aug. 1989, pp. 467–474.